Tikrit Journal of Engineering Sciences (2024); 31(1): 236-250
DOI: http://doi.org/10.25130/tjes.31.1.20

IRAQI Academic Scientific Journals

ISSN: 1813-162X (Print); 2312-7589 (Online)
Tikrit Journal of Engineering Sciences
available online at: http://www.tj-es.com

TJES Tikrit Journal of Engineering Sciences

Kinetic Analysis of Catalytic Dry Reforming of Methane Using Ni-ZrO2/MCM-41 Catalyst

Maha Al-Ali *, Alfaisal Aljbory, Ghassan H. Abdullah
Department of Chemical Engineering, College of Engineering, Tikrit University, Tikrit, Iraq.

Keywords:
Reaction Kinetic; MCM41; Nickel-Based Catalyst; Dry Reforming of Methane; Hydrogen; Activation Energy.

Highlights:

- *New catalyst was prepared with high activity in CDRM reaction.*
- *MCMZ provided high conversions with 89 and 91% for CH_4 and CO_2, respectively.*
- *The optimal CDRM reaction temperature was 800 °C.*
- *Two new models present CH_4 and CO_2 conversions can predict the rate of catalyst activity with very high accuracy.*

ARTICLE INFO
Article history:

Received	05 Aug.	2023
Received in revised form	26 Aug.	2023
Accepted	30 Sep.	2023
Final Proofreading	31 Jan.	2024
Available online	12 Mar.	2024

Citation: Al-Ali M, Aljbory A, Abdullah GH. **Kinetic Analysis of Catalytic Dry Reforming of Methane Using Ni-ZrO2/MCM-41 Catalyst**. *Tikrit Journal of Engineering Sciences* 2024; **31**(1): 236-250. http://doi.org/10.25130/tjes.31.1.20

**Corresponding author:*
Maha Al-Ali
Department of Chemical Engineering, College of Engineering, Tikrit University, Tikrit, Iraq.

Abstract: This work investigates the kinetics of catalytic dry reforming of methane (CDRM) to produce hydrogen gas using nickel-based catalysts. A new catalyst was prepared, Ni-ZrO2@MCM-41 (MCMZ) and used in the CDRM reaction. The textural, physical, and morphological scans are used to characterize the prepared catalyst. The performance of the newly prepared catalyst in terms of temperature effects and long-term stability is assessed. The reaction activation energy is studied as well. The outcomes of this study revealed that the MCMZ provided the highest conversion values for CH_4 and CO_2, with 89 and 91%, respectively. The optimum reaction temperature to achieve the highest syngas conversion was 800 °C. In addition, two new models that present CH_4 and CO_2 conversions for MCMZ as a function of reaction time to predict the rate of catalyst activity were built with very high accuracy. It was found that the activation energy was within the expected limits. Finally, the constants and reaction rate were determined. To conclude, this research creates a new catalyst with high performance to enhance hydrogen gas production from methane with carbon dioxide that contributes significantly to the field of yielding alternative energy sources.

دراسة حركية التفاعل الجاف للميثان باستخدام عوامل مساعدة من النيكل

مها العلي، الفيصل الجبوري، غسان حمد عبدالله

قسم الهندسة الكيمياوية / كلية الهندسة / جامعة تكريت / تكريت – العراق.

الخلاصة

في هذا العمل، تم دراسة حركية الإصلاح التحفيزي الجاف للميثان لإنتاج غاز الهيدروجين باستخدام عوامل مساعدة جديدة مبنية على مادة النيكل. تم تحضير عوامل مساعدة مطورة جديدة وهي: Ni-ZrO_2@MCM-41 لتستخدم في هذا التفاعل المذكور اعلاه. تم استخدام فحوصات التركيبية والفيزيائية والشكلية لتوصيف العامل المساعد المعد. تم تقييم أداء العامل المساعد المُحضر الجديد من حيث تأثيرات درجة الحرارة والاستقرار طويل المدى. كما تم دراسة طاقة تنشيط التفاعل أيضًا. اثبتت نتائج هذه الدراسة أن Ni-ZrO_2@MCM-41 يوفر أعلى تحويل للميثان وثاني أكسيد الكربون بنسبة ٨٩ و٩١٪ على التوالي. ان درجة الحرارة المثلى للتفاعل لتحقيق أعلى تحويل للغاز الناتج (الهيدروجين) هي ٨٠٠ درجة مئوية. بالإضافة إلى ذلك، تم بناء نموذجين رياضيين جديدين يمثلان حركية تفاعل CDRM بدقة عالية جدًا. كما وجد أن طاقة التنشيط هي ضمن الحد المقبول والمقدر بـ ٢٩ kJ /mol. أخيرًا، تم تحديد معدل التفاعل. نستنتج، ان هذا البحث قد صنع عامل مساعد جديدً بكفاءة عالية لإنتاج غاز الهيدروجين من الميثان والذي يمكن أن يساهم بشكل كبير في مجال إنتاج مصادر بديلة للطاقة.

الكلمات الدالة: حركية التفاعل، MCM41، عامل مساعد أساسه النيكل، إصلاح جاف للميثان، الهيدروجين، طاقة التنشيط.

1.INTRODUCTION

The most prominent greenhouse gases that dramatically increase are carbon dioxide, methane, hydrofluorocarbons, nitrous oxide, hydrochlorofluorocarbons, and ozone in the lower atmosphere. These gases, particularly carbon dioxide and methane emissions, are naturally released into the atmosphere. These two gases are identified as the main sources of global warming and, hence, climate change [1, 2]. In addition, energy consumption is increasing because of population growth and improved living conditions resulting in negative environmental outcomes via global warming from emitted greenhouse gases (GHG). The quality of life in technologically advanced communities has always been energy-dependent, and with the rapid growth of the population, energy demand/consumption is estimated to increase by 57% by 2030. The dependence on fossil fuels and biogas, mainly to meet worldwide energy demand, has increased GHG emissions. Consequently, human activities have markedly increased greenhouse gases' atmospheric concentration. Therefore, the necessity to limit the emission of greenhouse gases and transform these gases into more beneficial products is essential. Studies have been conducted to lower this undesirable impact and increase the production of syngas (H_2+CO) as an alternative fuel source. Hydrogen is one of the fuel sources and is considered environmentally friendly [3, 4]. Syngas, or particularly hydrogen gas, can be produced using various methods. Pham et al. [5] showed that the dry reforming of the methane process was a productive process to yield the syngas, where they got 77 and 87% conversion of CH4 and CO2, respectively, at 700 °C. Another study implemented by Zhang et al. [6] reached approximately 100% selectivity of syngas production with a fed ratio 2:1 of H2/CO at 500 °C using a nickel-based catalyst in the dry reforming of methane process. Dry reforming methane is a prospective process to change the two greenhouse gases, i.e., CH_4 and CO_2, into syngas (H_2/CO) [4, 7]. Methane is the major component of natural gas, widely used in producing hydrogen or syngas using different catalysts, heating methods, and operating conditions [8, 9]. Since the 1980s, the dry reforming of methane or catalytic carbon dioxide reforming of methane (CDRM), has gotten extensive attention from environmental, economic, and industrial implications due to the efficient exploitation of these two GHGs to produce the syngas with appropriate ratios (H2/CO) [3, 10]. CDRM is an endothermic reaction occurring at very high temperatures, requiring an efficient heating source [10].

$$CO_2 + CH_4 \leftrightarrow 2CO + 2H_2 \qquad \Delta H_{298k} = 206\ kJ/mol \qquad \textbf{(1)}$$

According to the endothermic nature of CDRM, which needs high temperatures for activity, considerable energy consumption, and high operational costs, the suitability of various catalysts for CDRM has been carefully examined [11, 12]. The fundamental challenge in producing syngas through CDRM is selecting the proper catalysts considering their activity, product selectivity, stability, and cost. The base metals are used in the CDRM as an inexpensive and abundant alternative to noble metals. However, they are rapidly deactivated due to catalyst sintering, coke production, and deposition on the catalyst surface. Thereby, they are uneconomically viable for use in large-scale industrial applications [11, 12]. Accordingly, the need to use an alternative catalyst that is available, efficient with high activity, and cost-effective in industrial applications is important. Compared to the noble metals and metal-based catalysts, it is found that nickel-based catalysts are more economical and appropriate for the CDRM process's industrial application due to the cost-effectiveness, high performance, and stability of nickel [13]. On the other hand, the deactivation of nickel-based catalysts and low stability due

to coke deposition (CO_2 reaction with C to form CO) and active metal sintering of catalysts are still major problems of these catalysts [14]. These obstacles can be treated in different ways. For instance, selecting an active metal that interacts with the support, adding promoters with essential characteristics, reducing particle size, evaluating the capability of several combinations of metal and support, and varying the pretreatment and preparation method [15]. For example, adding a promoter to the catalyst, such as MgO (strong Lewis base), improves the CO_2 chemisorption, thereby decreasing the coke deposition [16]. Also, Deng et al. [17] have used boron nitride to coat Ni-based catalysts for dry methane reforming to enhance the carbon-forming resistance. Binti Rosdin et al. [18] used magnesium oxide and zirconium oxide as support to promote the nickel-based catalyst in the dry CDRM process. Similarly, magnesium oxide was used in promoting nickel-based catalysts by Al-Fatesh et al. [19]. These studies proved the significant effects of the support used with the nickel-based catalyst in CDRM reaction. Therefore, this project focuses on using nickel-based catalysts with new supporters in CDRM reactions. In this work, a mesoporous material was developed by the Mobil Oil Corporation. Mobil Composition of Matter No. 41 (MCM41) is used as a catalyst supporter with the active material of NiZrO to prepare a new catalyst. This catalyst is used in the CDRM to improve the reaction conversion rate and production yield of hydrogen gas, which is selected as the most cost-effective, readily available, and more appropriate for heating than other catalysts. The chemical kinetics of this reaction using the newly prepared catalyst are investigated, and the reaction constants and rate are determined. The minimum energy required for the CDRM reaction is presented by calculating the activation energy of this reaction. Thus, this research aims to investigate the kinetics of the CDRM reaction to express the system performance and behavior using a newly prepared catalyst in planned operating conditions to produce an environmentally friendly energy source with reasonable conversion to be used in the industrial design and simulation.

2.METHODOLOGY

2.1.Materials

The methane was brought from the laboratories of the North Refineries Company in Baiji within the specifications attached in Table 1. Carbon dioxide, nitrogen, helium gases, and hydrogen gases were purchased from a local provider. The properties of those gases are tabulated in Table 1.

2.1.1.Catalysts Active Components and Support Material

Nickel nitrate hexahydrate and zirconium nitrate hexahydrate were used as the active materials in the catalyst preparations. Ethanol hydroxide was used as an emulsion breaker. Cyclohexane and ethylene glycol were used as solvents, while ammonium hydroxide was used as a pH stabilizer. More details about these materials are provided in Table 2. (MCM-41) is a mesoporous material belonging to a family of aluminosilicate and silicate solids, which is suitable to be used as catalysts and catalyst supports. MCM-41 has a hierarchical structure based on a regular arrangement of cylindrical mesopores ranging from 2 to 6.5 nm in diameter, see Fig. 1. MCM-41, used in this work, was a white powder of size ranging from 100 to 1000 nm with more than 850 m^2/g BET surface area, a 3.4 nm average pore diameter, and ≥0.75 cm^3/g pore volume [20].

Table 1 Properties of the Gases Used in Dry Reforming of Gases Used in the Reaction.

Gas name	Molecular weight (g/mol)	Purity (%)	Density (kg/m^3)	Boiling point (°C)	Melting point (°C)	Vapor pressure (kPa)	Viscosity (CP)
CH_4	16.04	89 %	0.656	−161.50	−182.5	6294.9	0.01107
CO_2	44.0095	92%	1.795	-78.464	-78.464	6450.0	1.495
N_2	14.0067	98%	1.25	-78.464	-195.8	3399.1	0.01695
H_2	2.016	98%	8.98	-252.87	-259.16	2916.5	0.009

Table 2 Active Components Used in this Study in Preparation of the Catalyst.

Chemicals	%Purity	Function	Supplier/Source
$Ni(NO_3)_2.6H_2O$	98.2	Active metal	Local provider
$Zr(NO_3)_4.6H2O$	97.5	Active metal	Local provider
C_2H_6OH	99	Micro-emulsion system breaker	Sigma-Aldrich, Germany
C_6H_{12}	98	A solvent of active materials	Sigma-Aldrich, Germany
$(C_2H_4O)n+H_2O$	---------	A solvent of active materials	Sigma-Aldrich, Germany
NH_4OH	100	Stabilizing pH to 7	Local provider

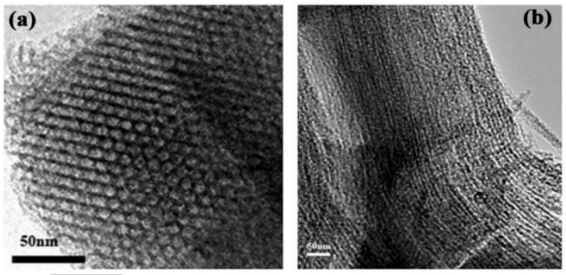

Fig. 1 MCM-41 Structure (a) Along the Channel Direction and (b) Perpendicular to the Channel Direction [21].

2.2.Method

2.2.1.Catalyst Preparation

Preparing the catalysts included fabrication using a one-pot method [22, 23]. MCM-41 was used as catalyst support. During the synthesis of MCM-41, a rod-shaped micelles surfactant of cetyltrimethylammonium bromide was added to the synthesis solution. Silica was added to coat the surfactant, condensed the silanol groups, and bridged the oxygen atoms with silicon atoms to form the MCM-41 [24]. A 1.25 gm of nickel nitrite, $Ni(NO_3)_2.6H_2O$, and 1.86 gm of zirconium nitrate, $Zr(NO_3)_4$, were dissolved in 50 ml of deionized water. A magnetic stirrer was used to stir the last solution for one hour at room temperature to get the saturated solution. Then, the solution was directly poured into 450 ml of polyethylene glycol and cyclohexane mixture with continuous stirring for 20 h at 40 °C. After that, 5 ml of concentrated ammonia solution (28 wt% NH_3) was promptly added into the first aqueous solution and incessantly stirred for 3 h. Moreover, 50 ml of deionized water containing 4.25 gm MCM-41 was added slowly dropwise with continuous stirring at 40 °C for 48 h. Later, 50 ml of ethanol hydroxide was added to the solution and centrifuged for 10 min at 5,000 rpm [24]. The initially obtained Ni-ZrO_2@MCM-41 nanoparticles were collected for the next step of drying and calcination. The collected Ni-ZrO_2@MCM-41 was dried in a furnace at 60 °C for 18 h, calcined at 600 °C for 3 h, and then constantly calcined at 800 °C for 3 h atmospheric pressure [24].

2.2.2.Characterization of the Catalyst

X-ray diffraction (XRD) patterns of the prepared catalyst samples were determined using Bruker AXS D4 Endeavour with CuKα radiation in Rigaku Smart Lab XRD at 19 Mayis University, Advanced Technology Research, and Application Center, Turkey. About 1 - 2 g of sample was placed on a specimen holder at room temperature and tested over a 2θ range (5 – 90 degrees) using a wavelength of 1.5406 Å and CuKα1 radiation at 40 kV and 35 mA. The crystalline structure and composition of the MCMZ were characterized using the XRD. Using the multipoint surface area analysis method, Brunauer-Emmett-Teller (BET) was used to determine the specific surface area SBET, total pore volume, and micropore volume of catalysts. The test was conducted in Quanta chrome Instrument v5.2 (Hitit University, Turkey). A catalyst powder of 0.274 g was placed in a sample cell and heated to 90 °C. The temperature was kept constant for the first hour of the test and then raised to 350 °C for 2 h. A scanning electron microscope (SEM) imaging for MCMZ was performed to estimate the morphology of the prepared catalyst using a JeolJsm-7001f scanning electron microscope (19Mayis University/Advanced Technology Research and Application Center, Turkey). A catalyst samples test was conducted by scattering a small amount of catalyst powder on double-sided adhesive tabs on Al stubs. Later, it was coated under vacuum with a carbon thin layer (~30 nm) at 2.0 kV and 25 mA. Various images were collected for further analysis. Lastly, transmission electron microscopy (TEM) was used with a very short electron beam through a thin specimen to form high-resolution images of samples on the nanoscale. The TEM observation was conducted using a Zeiss-EM10C-100KV transmission electron microscope accelerating voltage (19Mayis University/Advanced Technology Research and Application Center, Turkey). All TEM images were taken at 200 000 magnifications. The catalyst particle size distribution measurement calculations were executed using the Image-Pro software.3.4 Design and Manufacture of the Project System.

2.2.3.Reactor Set-up

A fixed bed reactor (40 cm height, OD 10 mm, and ID 6 mm) working at reaction heating temperature, reached 850 °C (max) with a heat rate of 15 °C/min was built and worked efficiently Fig. 2. The reactor comprised a stainless-steel mesh cup of 2 to 5 nm size. This cup was designed to contain the catalyst powder in the middle of the reactor. The reactor furnace was built using electric heaters with a capacity of 3000 W wrapped in a spiral to turn them around and made them surround the reactor, then enclosed with a stainless-steel cylinder. The system specifications are reported in Table 3.

Table 3 Technical Parameters of the Fixed-Bed Tubular Reactor.

Reactor Specifications	
Model	Fixed Bed Tubular Reactor
Temperature	Up to 850 °C
Heating type	Electrical furnace
Mode of temp. control	PID
Volume	11.3 ml
Covering material	Stainless steel
Power of Heating	3000 W
Accuracy of temp. control	± 15°C
Power supplied	220 V
Wire of the furnace	$Cr_{20}Ni_{80}$
Temp. sensor	Thermocouple (K-type)

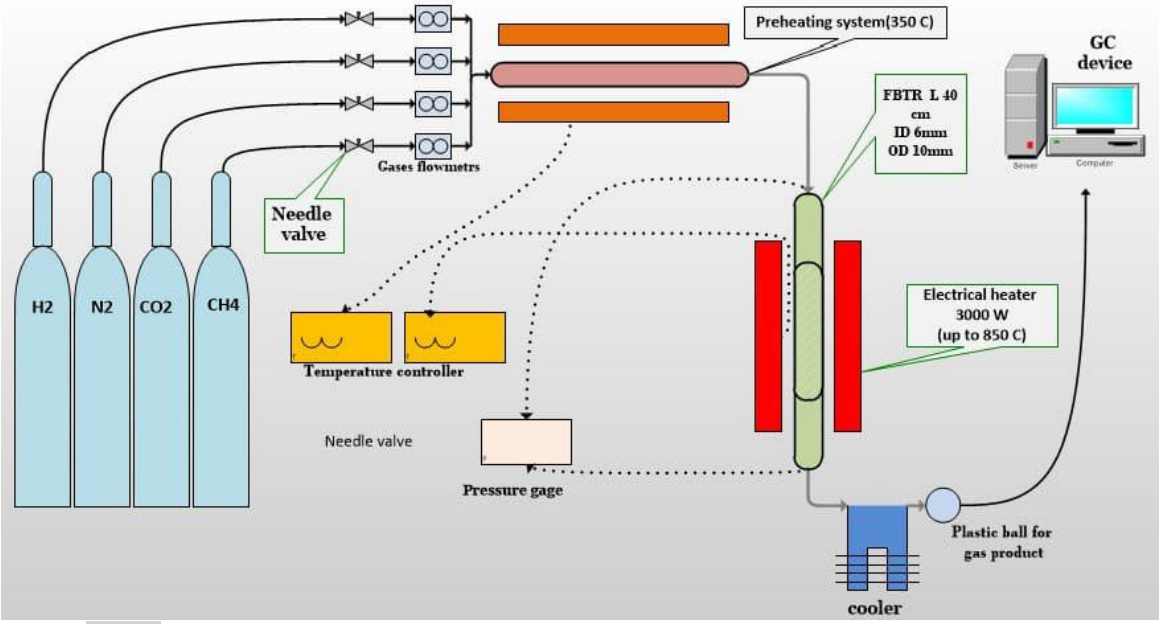

Fig. 2 A Schematic Diagram of the Catalytic Dry Reforming of the Methane System.

2.2.4.Experimental Procedure

100 mg of catalyst powder MCMZ (NiZrO2@MCM-41) was placed in the reactor bed using the mesh cup 5000 in the middle of the reactor in a disk shape. To activate the catalyst in the reaction, hydrogen gas flowed with 50 ml/min for 20 min at 800 °C. Then, the gases were supplied to the reactor at a pressure of 1 atm and a rate of 80 ml/min at a ratio N_2:CH_4:CO_2 of 40:20:20 ml/min. The flow was controlled using the flowmeter for each gas; the initial heating temperature was set at 450 °C, and the reactor furnace temperature was set at 500 °C. Samples were withdrawn from the gas products of the reaction and collected using plastic balls to be tested using the gas chromatograph (GC) device. GC was used to examine the conversion rate of methane gas by injecting samples of the reaction product into the GC device. For the first experiment and after 120 minutes of operation, the reactor vessel was washed firstly using ethanol solution and secondly using deionized water and then was left until dried and prepared for the next experiment. These steps were repeated, using temperatures of 600, 700, and 800 °C; samples were taken simultaneously after 20 minutes and examined using the GC. All previous steps were repeated, and samples were taken 10 hours after the reaction to approve the activity/performance of the catalyst at different reaction temperatures. The reactor was re-cleaned and re-filled with 100 mg of the first catalyst, and the activation process was conducted using hydrogen gas. The reactor was fed with gases with the same proportions in step number 1 but at a constant temperature (800 °C), using different intervals of time 2, 10, 18, 20, 22, 28, 30, 32, 38, 40, 42, 48, 50, 52, 58, and 60 hours. 10. The results were analyzed by measuring the percentage of methane remaining after conducting the reaction and knowing its conversion. The operating parameters used in this work are illustrated in Table 4.

Table 4 Variable Parameters Used in Catalytic Dry Reforming of Methane Process.

Variables	Variables number	Values
Catalyst	1	MCMZ
Temperature (°C)	4	(500, 600, 700, 800)
Reaction time (h)	3	(2, 10, 10 ~ 60)

2.3.Reaction Kinetics Theory

Kinetic studies for the fixed bed reactor running a dry reforming reaction of CH_4 with CO_2 under differential conditions were managed in the same reactor system. Although the CDRM reaction thermodynamics is well understood, the information about its mechanism and kinetics is still vastly questionable [25]. In this research, the kinetics of the CDRM reaction is determined. CDRM belongs to a considerably complex reaction, Eq. (1). However, Eqs. (2)-(6) show the importance of the other reactions of all product composition obtained from the main reaction, Eq. (1). The reaction kinetics is highly related to the feed composition and reaction conversion [26].

$$CO_2 + H_2 \leftrightarrow CO + H_2O \quad \textbf{(2)}$$

$$O_2 + 4H_2 \leftrightarrow CH_4 + 2H_2O \quad \textbf{(3)}$$

$$CH_4 + H_2O \leftrightarrow CO + 3H_2 \quad \textbf{(4)}$$

$$CH_4 \leftrightarrow C + 2H_2 \quad \textbf{(5)}$$

$$2CO \leftrightarrow C + CO_2 \quad \textbf{(6)}$$

Recently, another suggested mechanism points to the CH_4 decomposition to carbon atoms in elementary H-construction steps, quickly converted into H atoms to be extracted from CH_4, the most relevant step kinetically [27]. CO2 is dissociative adsorbed as CO and O on the

catalyst's surface. The CDRM reaction equilibrium to produce the synthesis gas is represented by Eq. (1) and effectively affected by the instantaneous occurrence of the RWGS reaction, Eq. (2). Some researchers set that, during CDRM, the RWGS reaction occurs closely to thermodynamic equilibrium [28, 29]. to ease the calculations, other researchers considered that the CDRM reaction is at equilibrium in the kinetic consideration [30]. Bradford and Vannice have considered the first assumption of RWGS reaction in their calculations over a wide range of temperatures [31]. The present investigational outcomes showed that the conversion of CO_2 is higher than CH_4 due to the RWGS equilibrium. The measured selectivity H_2/CO ratios were calculated by the stoichiometric equation Eq. (7). This reaction indicates that the reaction of CDRM is affected by the instantaneous happening of the RWGS reaction [32].

$$H_2/CO = \left(3 - \frac{r_{CO_2}}{r_{CH_4}}\right) \Big/ \left(1 + \frac{r_{CO_2}}{r_{CH_4}}\right) \quad (7)$$

where r_{CH_4} and r_{CO_2} are the experimental rates of CH_4 and CO_2 conversions, respectively. The differential analysis method was used to determine the reaction rate equation, including the reaction constant and order. In this method, the system was assumed to be isothermal, and the pressure drop was negligible. Also, consider CH_4, CO_2, CO, and H_2 in Eq. (1) as A, B, C, and D, respectively [33].

$$A + B \leftrightarrow 2C + 2D \quad (8)$$

$$F_{A_0} = \frac{v_A x \rho_A}{MW_{t_A}} \quad (9)$$

$F_{A_0} = 0.0492\, mol/hr$;
$F_{B_0} = 0.0489\, mol/hr$
$\theta_B = F_{B_0}/F_{A_0} = 0.993 \cong 1.0$

$$\delta = \frac{c}{a} + \frac{d}{a} + \frac{b}{a} - 1 = \frac{2}{1} + \frac{2}{1} + \frac{1}{1} + 1 = 2 \quad (10)$$

$y_{A_0} = y_{B_0} = 0.5; \qquad \in = y_{A_0}.\delta = 1$
$C_{A_0} = \frac{F_{A_0}}{v} = 0.041 \frac{mol}{l}$

$$F_A = F_{A_0}(1 - x) \quad (11)$$

$$F_B = F_{A_0}\left(\theta_B - \frac{b}{a}x\right) \quad (12)$$

$$F_C = F_{A_0}\left(\theta_C + \frac{c}{a}x\right) \quad (13)$$

$$F_D = F_{A_0}\left(\theta_D + \frac{d}{a}x\right) \quad (14)$$

$$F_D = F_C = F_{A_0}(2x) \quad (15)$$

$$C_A = \frac{F_{A_0}}{v}(1 - x) = C_{A_0}(1 - x) \quad (16)$$

$$C_B = \frac{F_{B_0} - \frac{b}{a}F_{A_0}x}{v} = C_{A_0}\frac{(1 - x)}{(1 + x)} \quad (17)$$

$$C_C = \frac{F_{C_0} - \frac{c}{a}F_{A_0}x}{v} = C_{A_0}\frac{(2x)}{(1 + x)} \quad (18)$$

$$C_D = \frac{F_{D_0} - \frac{d}{a}F_{A_0}x}{v} = C_{A_0}\frac{(2x)}{(1 - x)} \quad (19)$$

$$\frac{-r(a)}{a} = \frac{-r(b)}{b} = \frac{r(c)}{c} = \frac{r(d)}{d} \quad (20)$$

$$r(c) = 2.(-r(a)) \qquad -r(a) = \frac{FAo\ X}{\triangle W} \quad (21)$$

For forward reaction [33, 34]:

$$\acute{r}(c) = kC_A^{\alpha}C_B^{\beta} \quad (22)$$

$$C_B \rightarrow \check{K} = kC_B^{\beta} \ ; \ \acute{}r(c) = \check{k}C_A^{\alpha} \quad (23)$$

$$ln\acute{r}(c) = ln\check{k} + \alpha lnC_A \quad (24)$$

For backward reaction, the concentration C equals D [33]:

$$2C + 2D \rightarrow A + B \quad (25)$$

$$-\acute{r}(c) = k_n\, C_C^{\gamma} \quad (26)$$

$$ln(-\acute{r}(c)) = ln\, k_n + \gamma lnC_C \quad (27)$$

3.RESULTS AND DISCUSSION

3.1.Catalyst Characterization

3.1.1.BET Results

BET test shows the presence of a mesopore structure in the range (30 to 40 nm) for the MCMZ catalyst according to the silica particle accumulation. The specific surface area of MCMZ was 143 m^2/g. The pore volume of MCMZ was 1.328 $cm^3.g^{-1}$. These outcomes are compatible with the results earlier reported in the literature for this type of catalyst with a core-shell structure [35]. For example, Zhang et al. [36] and Liu et al. [24] determined the BET surface area and pore sizes of their catalysts used in CDRM reactions. BET test results are illustrated in Table 5.

Table 5 The Catalyst Surface Area, Pore Volume, and Average Radius.

Catalyst	BET Surface Area (m2/g)	Total Pore Volume (cm3/g)	Radius Average (nm)
MCMZ	143.122	1.328	1.85608

3.1.2.SEM Results

The MCMZ catalyst morphology prepared in the present work was considered by scanning electron microscopy (SEM). MCMZ's SEM imaging and its constituents are shown in Fig. 3. It is observed that MCMZ particles had few large particles with grainy and crumbly shapes,

and some of them were relatively small in spherical or semi-spherical shape, and other very small particles with irregular morphology and core-shell shape and cleaved surfaces [35]. This result is consistent with Barbosa et al. [37] and Sukri et al. [38]. Both researchers showed that the micrographs of their prepared catalyst revealed the coral-reef-like structure in irregular shapes along with cleaved surfaces [37, 38].

3.1.3.TEM Results

TEM was used to image nanoparticles and the crystallinity of MCMZ. The average crystallite size for MCMZ was 7.5 nm (estimated by applying ImageJ software). This finding agrees with that obtained from XRD patterns, which refer to a wider peak width and a smaller crystallite particle size [18]. This test proves that adding ZrO_2 to the MCM-41 support produces finer morphology. As shown in Fig. 4, most Ni nanoparticles were fitted between the zirconia shell and silica core [39]. Thus, TEM results are compatible with Yang et al. [40]. The study explored the high dispersion of Zr and Ni particles in the molecule sieve and support, respectively [40].

3.1.4.XRD Results

Figure 5 illustrates the XRD patterns of the MCMZ catalyst. The XRD pattern of the MCM-41 revealed several peaks between the angle (2θ) 20 to 40° with different positions and intensities. The appearance of sharp peaks at 23.5, 30, and 34.5 ° indicated the MCM-41 crystalline nature. While the broad peaks refer to the amorphous nature [41, 42], which verifies the results of the present work. The diffraction peaks at 23.5, 30, 34.5, 50.3, and 64° are indexed to the nickel phyllosilicate $Ni_3Si_4O_{10}(OH)_2.5H_2O$ [43, 44]. These outcomes agree with Yang et al.'s [40] investigation of dry reforming of methane, where they used Ni/ZrO2Sin@MCM-41 as a catalyst. In particular, the peak at 13 of MCM-41 and other peaks at 36, 42, and 64° of nickel oxides or nickel phyllosilicates [40]. Taherian et al. [45], who used Ni-MgO-MCM-41, showed similar results due to the effect of metal oxides on MCM-41.

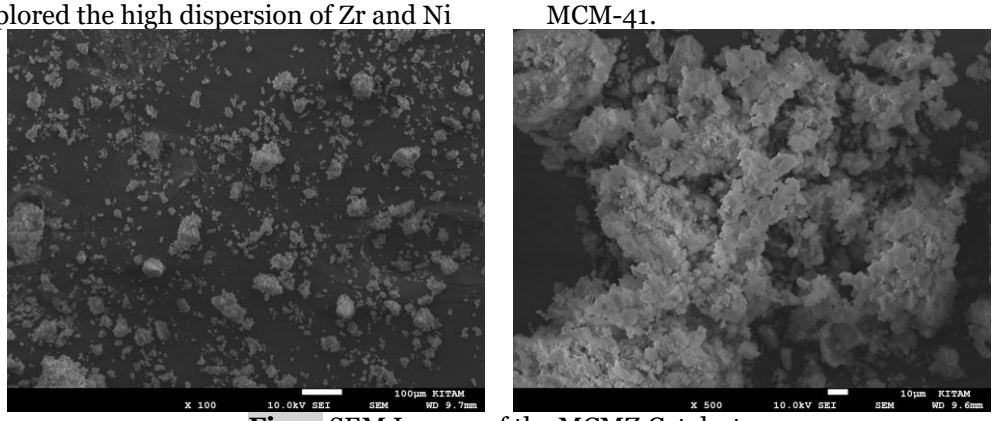

Fig. 3 SEM Images of the MCMZ Catalyst.

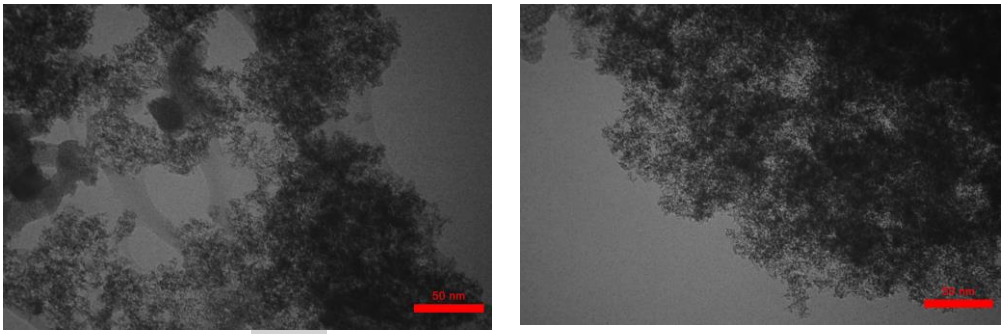

Fig. 4 SEM Images of the MCMZ Catalyst.

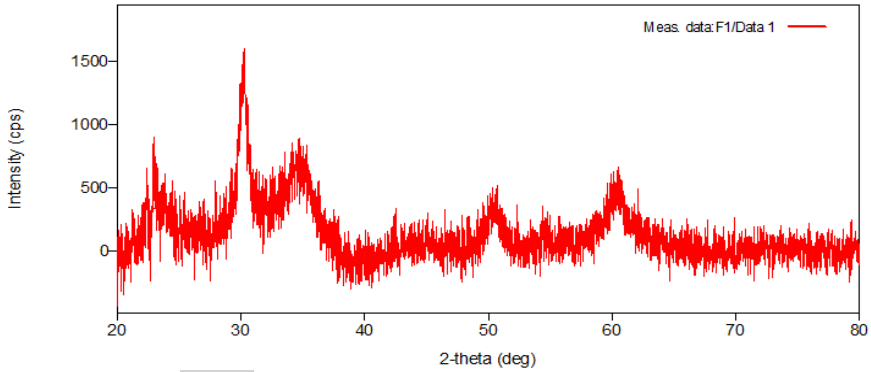

Fig. 5 XRD Patterns of the MCMZ Catalyst.

3.2.CDRM Catalytic Performances

3.2.1.Temperature Effect

The effectiveness of the catalyst and its ability to convert methane to syngas at different temperatures (500, 600, 700, and 800 ˚C) during constant intervals of time were examined. This section displays the temperature effect on the reaction conversion using MCMZ. The tests were performed for 2 h (Fig. 6) and 10 h (Fig. 7) to explore the optimum temperature with good performance. The variations in conversion percentages of CH_4 and CO_2 with increasing temperatures in the CDRM using MCMZ during 2 h are shown in Fig. 6. It is shown that the conversion percentages of CH_4 and CO_2 at 500 ºC were 20 and 25%. These percentages intensely increased to 55 and 82% for CH_4 and 61 and 84% for CO_2 when the temperature increased to 600 and 700 °C, respectively. Progressively, the conversions of CH_4 and CO_2 increased to their highest at 89 and 91%, respectively, with increasing reaction temperature to 800 ºC after 2 h of reaction. Hence, the methane and carbon dioxide conversion percentages using MCMZ were significantly improved with the rise in reaction temperatures because the CDRM was an endothermic reaction highly required in high-temperature reactions [24]. These results demonstrated that methane and carbon dioxide conversions achieved their highest levels at 800 °C during two hours of reaction. MCMZ provides the highest conversion values for CH_4 and CO_2 with 89 and 91%, respectively. On the other hand, Fig. 7 displays the CDRM experiment results conducted after 10 h using MCMZ. The reaction conversion percentage of CH_4 and CO_2 at 500 °C were 19 and 22%, respectively. These values of conversions jumped up to 52 and 59% at 600 °C and then increased to 78 and 81% at 700 °C for CH_4 and CO_2, respectively. While at the highest reaction temperature (800 °C), the conversions of CH_4 and CO_2 increased to 81 and 89%, respectively. From Figs. 6 and 7, it is noticed that the CO_2 conversion is slightly greater than the conversion of CH_4 and attributed to the reverse water-gas shift (RWGS) reaction of Eq. (1), ($CO + H_2O \leftrightarrow CO_2 + H_2$). In addition, it was found that the best reaction temperature ranges from 700 to 800 ˚C, where 800 ˚C was optimal according to the high reaction conversion rate. This finding is consistent with the results obtained from the study of Song et al. [46] when they used the catalyst MgO/Al_2O_3 support at 800 °C. They achieved conversions for CH_4 and CO_2 of 86% and 91%, respectively. Also, Lou [47] got 84% and 89% conversions of CH_4 and CO_2, respectively, when they used Ni/ZrO_2 at 700 °C.

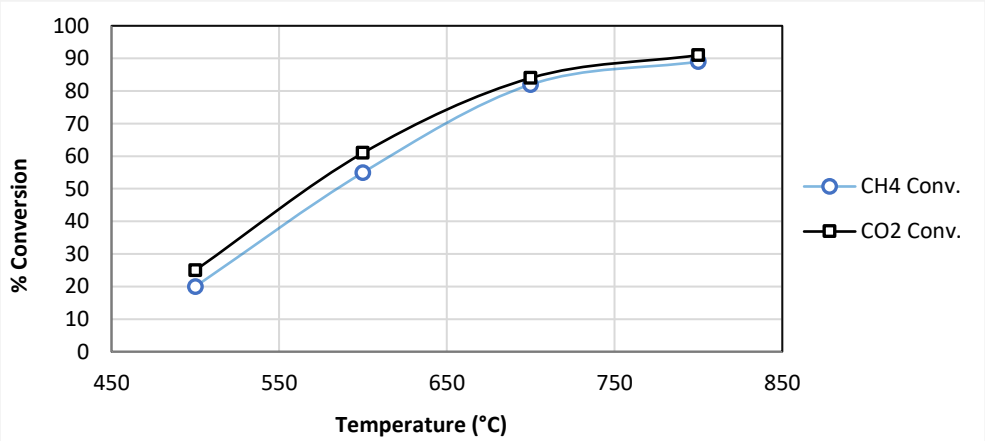

Fig. 6 CH_4 and CO_2 Conversion After 2h Using MCMZ Catalyst.

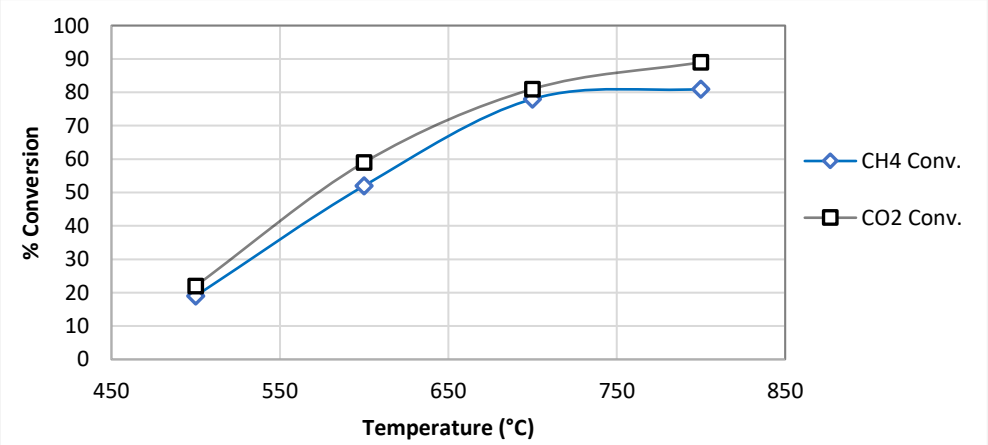

Fig. 7 CH_4 and CO_2 Conversion After 10h Using MCMZ Catalyst.

3.2.2.Long-Term Stability Test of MCMZ During the CDRM

Catalyst stability is a substantial consideration of the catalyst's functioning and performance, especially when using the catalyst in reactions with high temperatures. A catalyst with good stability means obtaining one that can resist carbon sintering and deposition at high temperatures and continue working with catalyst poisoning. Therefore, catalytic stability tests were performed in the present reactor with a 1:1 molar feed ratio of CH_4:CO_2 for both prepared catalysts. To explore the MCMZ catalyst's capabilities, a long-term stability test of the CDRM was conducted at 800 °C for 60 h. Fig. 8 displays the conversion changes of CH_4 and CO_2 versus reaction time using MCMZ catalyst. Fig. 8 shows that the conversion of CH_4 at 800 °C during the first hour of the reaction is 88%. Then, the conversion reduced gradually to reach its lowest 68% after 60 h. However, the highest CO_2 conversion within the first hour of reaction using MCMZ was 91%. The conversion slightly decreased to 79.8% after 60 h of reaction.

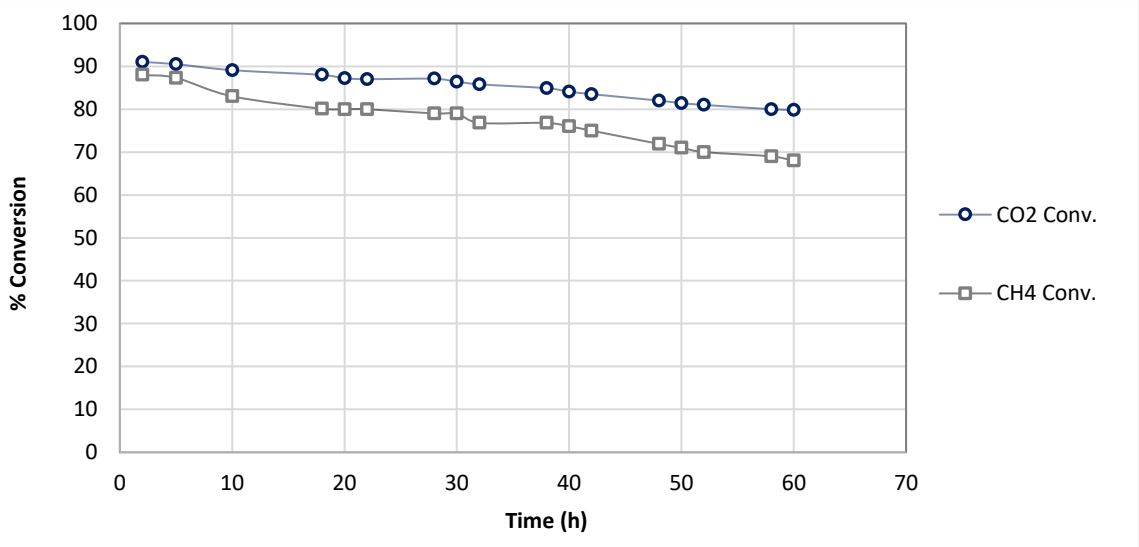

Fig. 8 CH_4 and CO2 Conversion Versus Time in Long-Term Stability Test of MCMZ Catalyst.

At 800 °C, it is observed that the MCMZ demonstrated low deactivation within a long-time reaction, estimated to be more than 60 h of reaction. This high stability of the catalyst signifies no serious impacts on the catalyst activity caused by the side reactions of the decomposition of CH_4 and the RWGS reaction. Thus, the MCMZ presents good stability during the CDRM reaction. The significant resistance of the prepared catalyst to the sintering and coking can be ascribed to the zirconium oxide and MCM-41 structure (core-shell structure). The high dispersion of Ni species with ZrO_2 maintains the resistance of Ni particles sintering [48] because ZrO_2 presents an obstacle that inhibits Ni from sintering by reducing the formation of nickel oxide [49]. In addition to the fact that ZrO_2 decreased the dissociation barriers of CO_2, it increased its adsorption energy [39]. As a result, the high dispersion of nickel particles due to the presence of zirconium in the MCMZ catalyst and, hence, the high desorption of hydrogen and adsorption energy of carbon dioxide, the MCMZ catalyst highly enhanced the CDRM reaction. In association with the present results, Zhang et al. [50] tested the stability of their prepared catalysts (mesoporous silica), which showed their highest stability by decreasing sintering and carbon deposition. Additionally, the rate of CH_4 and CO_2 conversions as a function of time using MCMZ catalyst can be represented by the linear Eqs. (28) and (29), respectively.

$$Conv_{CH4} = -0.003\ t + 0.877 \qquad R^2 = 0.968 \tag{28}$$

$$Conv_{CO2} = -0.002\ t + 0.916 \qquad R^2 = 0.983 \tag{29}$$

where $Conv_{CH4}$ is the rate of catalyst activity in terms of CH_4 conversion, $Conv_{CO2}$ is the rate of catalyst activity in terms of CO_2 conversion, and t is the CDRM reaction time (h). The parity plot in Fig. 9 (a) compares the experimental CH_4 conversion values with those estimated by the mathematical model in Eq. (28). The plot's R^2 value (0.984) indicates the goodness of fit of the predicted data to that obtained from empirical work. Similarly, the experimental values of conversion of CO_2 were compared to those estimated using Eq. (29) in a parity plot Fig. 9 (b). The very high R^2 values with (0.992) for this plot indicated that the created model in Eq. (29) is reliable in estimating the rate of CO_2 conversions using the MCMZ catalyst. Hence, both models, in Eqs. (28) and (29), match the empirical data.

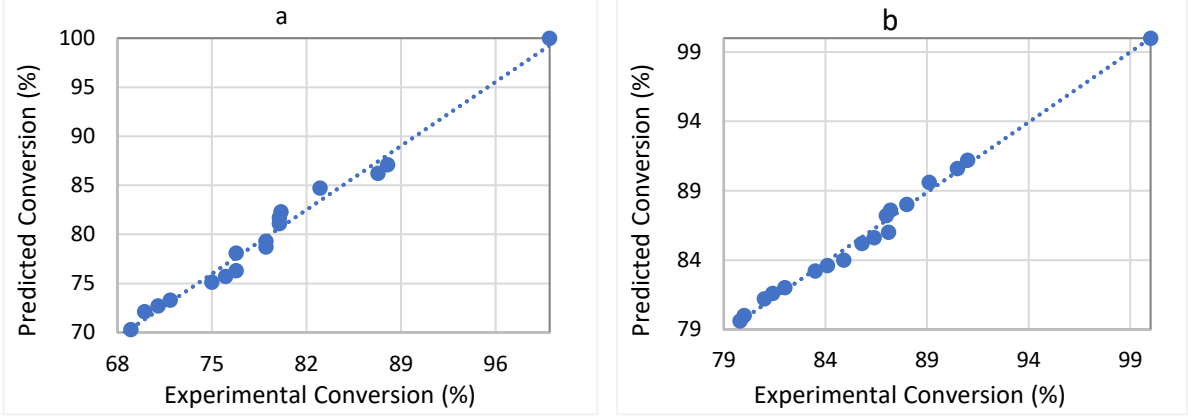

Fig. 9 Statistical Fit of the Proposed Models to Compare the Experimental with the Predicted Conversion Data of (a) CH_4 and (b) CO_2.

3.3.Kinetic Calculations for Dry Reforming of Methane Reaction

Equations (7) to (27) were used to determine the reaction constants, reaction rate, and concentrations of the CDRM reaction.

The equation of the CDRM reaction rate, from Eq. (1), can be written as Eq. (30):

$$A + B \leftrightarrow 2C + 2D \quad or \quad ((CO_2 + CH_4 \leftrightarrow 2CO + 2H_2))$$

$$-r(a) = k_m C_A^{\alpha} C_B^{\beta} - k_n C_C^{\gamma} \qquad \textbf{(30)}$$

For forward reaction, use Eqs. (22) to (24), and thus from Fig. 10 (a), which shows the correlation between lnŕ(c) and $\ln C_A$, the slope = $\alpha = 0.165$, and the intercept lnk_1=1.027.

$$\therefore k_1 = 2.793$$

To calculate β and C_B from the constant k_2:

$$\acute{r}(c) = k_2 C_B^{\beta} \qquad \textbf{(31)}$$

$$ln\acute{r}(c) = lnk_2 + \beta lnC_B \qquad \textbf{(32)}$$

From Fig. 10 (b), which shows the correlation between lnŕ(c) and $\ln C_B$, the slope $\beta = 0.154$, and the intercept $lnk_2 = 0.0786$.

$$\therefore k_2 = 1.082$$

Apply Eq. (22) to calculate k_m:

$$k_1 = k_m C_B^{\beta} \qquad \textbf{(33)}$$

$$\therefore k_m = \frac{k_1}{C_B^{\beta}} \quad ; \quad where\ k_1 = 2.793$$

$$k_m = \frac{2.793}{0.001932^{0.154}} = 7.311\ mol.\ l^{-2} gm_{cat}^{-1}.h^{-1}$$

$$\therefore k_m = 7.311\ \ mol.l^{-2} gm_{cat}^{-1}.h^{-1}$$

For backward reaction, the concentration C equals D, using Eqs. (25) to (27), and from Fig. 10 (c), which shows the correlation between lnŕ(c) and $\ln C_C$, the slope = 1.85, and the intercept $ln\ k_n = 1.28$.

$$\therefore k_n = 3.6\ mol.\ l^{-2}.gm_{cat}^{-1}.h^{-1}$$

The rate of reaction equation is:

$$-r(a) = k_m C_A^{\alpha} C_B^{\beta} - k_n C_C^{\gamma} \qquad \textbf{(34)}$$

$$-r(a) = 7.311\ C_A^{0.165}\ C_B^{0.154} - 3.6 C_C^{1.85} \qquad \textbf{(35)}$$

The close value of k_m was about 14.13 $mol.\,bar^{-2}.gm_{cat}^{-1}.h^{-1}$ by Barroso Quiroga et al. [26] when using the Langmuir-Hinshelwood for the DRM reaction at 800 °C.

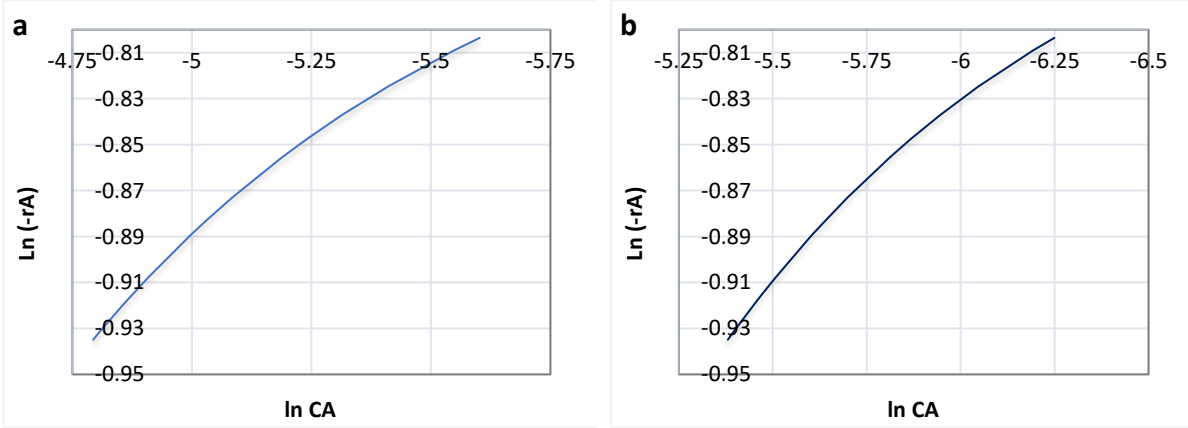

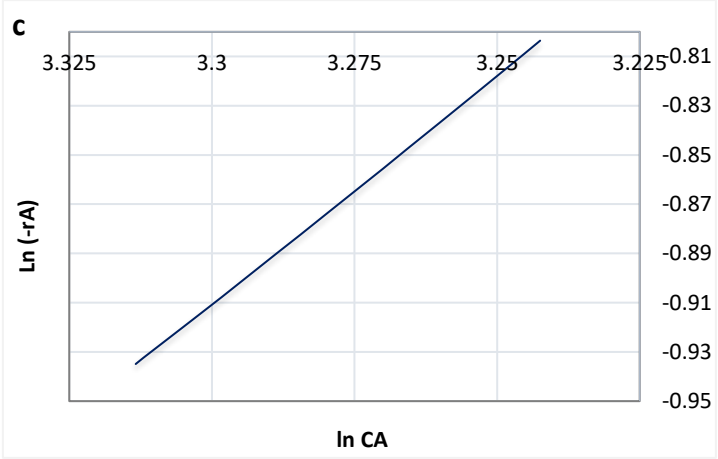

Fig. 10 Plot of ln ŕ(A) versus (a) ln C_A, (b) ln C_B, and (c) ln C_C.

The study of reaction kinetics for CDRM contributes to getting an appropriate reaction that can be favorable for academic and industrial fields. According to the investigational analysis, the obtained reaction kinetic model can predict the reactant conversion rate and related product formation [51]. It mainly interests industrial discipline since it can optimize the CDRM reaction, reactor design, and catalyst [51]. Similar studies were conducted in the literature using a linear regression model to predict the reaction rate, such as the kinetics study of CDRM over the Ca-promoted 1Coe1Ce/AC-N catalyst by Sun et al. [52]. In addition, Vertis et al. developed a kinetic model by linear reaction plot [53].

3.4.H_2/CO Ratio

For the product selectivity H_2/CO, according to Eq. (7), it is observed that the ratio of H_2/CO was about 0.97 within the first 2 hours of reaction and reached 0.90 over 40 hours to drop to 0.84 after 60 h of reaction using MCMZ catalyst, which is remarkably high, as shown in Fig. 11. Similar results were obtained in the CDRM reaction using a 5Nio.5Ce/MCM-41 catalyst by Al-Fatesh et al. [54]. This study showed that when the conversion was 90%, the selectivity of H_2/CO was approximately 1 after 330 min, and the selectivity of H_2/CO was 0.98 when the conversion dropped to 80% after 75 h of reaction [54]. Therefore, it can be concluded that adding ZrO_2 into the catalyst provided good catalytic activity and stability, resulting in a high H_2/CO ratio.

3.5.Activation Energy Calculations

The activation energy is the minimum rise in reactants' potential energy needed to transform the reactants into products. The activation energy reflects the energy transfer between reacting molecules that must be overcome [55]. Arrhenius equation (E_a) is applied to obtain the activation energy of the CDRM reaction [56]. Calculations on the reaction constants for forward reaction at four temperatures (500, 600, 700, and 800 ˚C) are performed. Also, the conversion was determined using the reaction rate equation. For the forward reaction, using equations (16, 17) and the reaction rate, Eq. (35):

$$-r(a) = \frac{FAo\ X}{\triangle W} \quad ; \qquad k = \frac{-r(a)}{C_a^{0.165} C_b^{0.154}}$$

From experimental data, the conversion rates of A at (500, 600, 700, and 800 ˚C) are shown in Table 6. Use Arrhenius Equation:

$$k = AExp^{-E_a/RT} \qquad \textbf{(36)}$$

where k is the reaction rate constant, A is the pre-exponential factor, E_a is the activation energy (kJ/mol), T is the temperature (K), and R is the gas constant ($8.314\ J/K.mol$) [56].

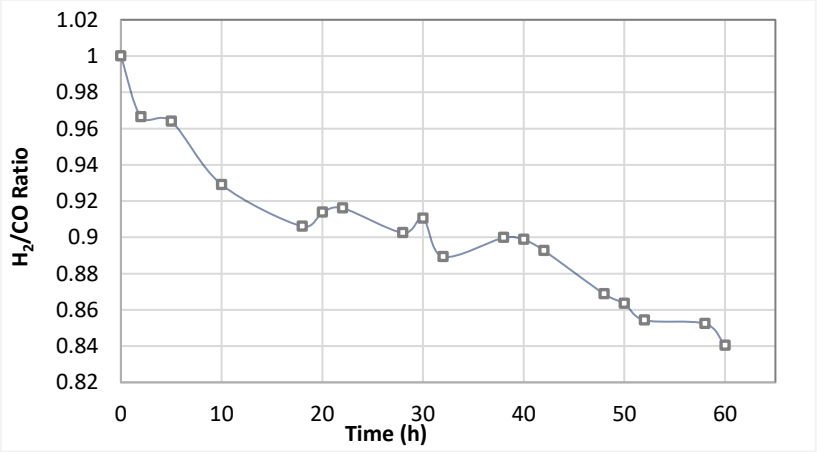

Fig. 11 The Selectivity (H_2/CO) of CDRM Reaction over Time.

Table 6 Conversion Rates of CH4 at Different Temperatures.

Temperature (°C)	Conversion (X)	C_A $mol.l^{-1}$	C_B $mol.l^{-1}$	$-r(a)$ $mol.gm_{cat}^{-1}.h^{-1}$	K $mol.l^{-2}.gm_{cat}^{-1}.h^{-1}$
500	0.25	0.0308	0.0246	0.123	0.386
600	0.61	0.0160	0.00993	0.300	1.207
700	0.84	0.0066	0.00356	0.413	2.252
800	0.91	0.0037	0.00193	0.448	2.954

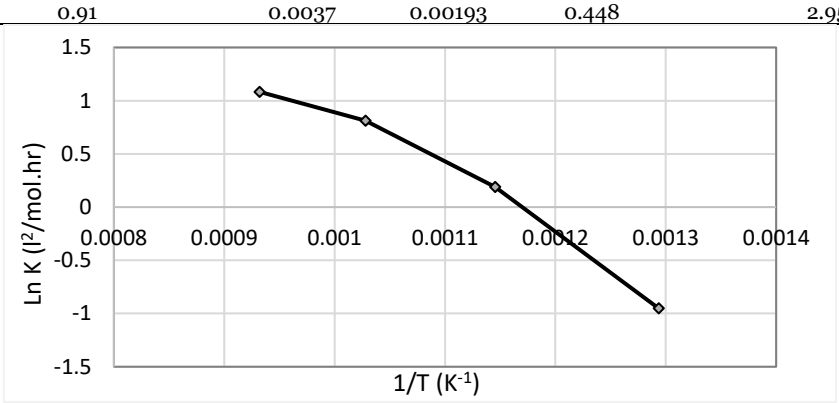

Fig. 12 CDRM Reaction Activation Energy.

$$lnk = -\frac{E_a}{R}\left(\frac{1}{T}\right) + lnA$$

From Fig. 12, the slope $-\frac{E_a}{R} = -5698.3$

The intercept $lnA = 6.55$

$\therefore E_a = 47.4\ kJ/mol \quad and \quad A = 698.6.$

It is well known that the apparent activation energy ranges from 29 to 306 kJ/mol [31]. Therefore, the result of the obtained activation energy with MCMZ is convenient with that stated in the CDRM reaction literature and confirms the catalyst's activity in this reaction (Fig. 12). Likewise, Zhang et al. [50] determined the apparent activation energy. They stated that the unique inverted conical pore structure in Ni/SiO_2 catalyst minimizes the apparent activation energy for CH_4 and CO_2 conversions, thereby reducing the energy needed to achieve the reaction [50]. Moreover, the kinetics study achieved by Li et al. [57] discovered that the lowest activation energy was 97.61 kJ/mol when Ni/CeO_2-H was used in the CDRM reaction among the Ni/CeO_2 catalysts. In general, the lower the activation energy, the quicker the reaction. On the other hand, a high activation energy will slow down the reaction [58].

4.CONCLUSIONS

In the present work, new Ni-based catalysts were prepared and used in the CDRM to produce syngas/H_2. MCM41 was used as a catalyst support to form Ni-ZrO_2@MCM-4. SEM, XRD, BET, and TEM scans of the catalyst revealed a good interaction between the MCM41 and the nickel particles. The conversion percent of the CDRM reaction increased with the increase in reaction temperature, where 800 °C was optimal. The MCMZ exhibited low deactivation, even after 60 h of reaction at 800 °C; thereby, the stability of MCMZ was great. The minimum energy required to accomplish the CDRM reaction was 47.4 kJ/mol, which is compatible with the activation energy obtained from the literature. The kinetics of CDRM reaction suggested the reaction rate, which can be expressed as: $-r(a) = 7.311\ C_A^{0.165}\ C_B^{0.154} - 3.6C_C^{1.85}$.

ACKNOWLEDGMENTS

The authors are grateful for the technical support provided by the Chemical Engineering Department, College of Engineering, Tikrit University. We appreciate the efforts of the technical staff of 19 Mayis University/Advanced Technology Research and Application Center, Turkey).

NOMENCLATURE

A	Pre-exponential factor
C_A, C_B, C_C	Concentration of species A, B, and C, respectively (mol/l)
C_{A_0}	Initial concentration of species A (mol/l)
E_a	Activation energy (KJ/mol)
F_{A_0}, F_{B_0}	Feed rate to the reactor (mol/h)
F_{A_f}, F_{B_f}	Effluent rate from the reactor (mol/h)
k_m	Forward Reaction constant (mol .l/ gm_{cat}. h)
k_n	Reversible reaction constant (mol .l/ gm_{cat}. h)
k	Reaction rate constant in Arrhenius equation
MW_{t_A}	Molecular weight for A (gm/mol);
R	Gas constant (8.314 J/K. mol)
ŕ(c)	Reaction rate of species C (mol/gm_{cat}. h)
T	Temperature (K)
X	Conversion for species A
y_{A_0}, y_{B_0}	mole fraction for species A, and B, respectively
Greek symbols	
α, β, and Y	Reaction order for species A, B, and C, respectively
v_A	Volume flow rate of species A (lit/h)
ρ_A	Density of species A (gm/lit)
∈	Emissivity
δ	Change in the total number of moles/moles of A reacted
θ_B	Moles of species B initially/moles of species A initial
ΔW	Catalyst weight (gm_{cat})
Subscripts	
CDRM	Catalytic dry reforming of methane
GHG	Greenhouse gases
MCMZ	Prepared catalyst
RWGS	Reverse water-gas shift

REFERENCES

[1] Cui Y, Liu Q, Yao Z, Dou B, Shi Y, Sun Y. **A Comparative Study of Molybdenum Phosphide Catalyst for Partial Oxidation and Dry Reforming of Methane**. *International Journal of Hydrogen Energy* 2019;**44**(23):11441-11447.

[2] Xu R, Chou L-C, Zhang W-H. **The Effect of Co2 Emissions and Economic Performance on Hydrogen-Based Renewable Production in 35 European Countries**. *International Journal of Hydrogen Energy* 2019;**44**(56):29418-29425.

[3] Kumari R, Sengupta S. **Catalytic Co2 Reforming of Ch4 over Mgal2o4 Supported Ni-Co Catalysts for the Syngas Production**. *International Journal of Hydrogen Energy* 2020;**45**(43):22775-22787.

[4] Charisiou ND, Siakavelas G, Tzounis L, Sebastian V, Monzon A BM, Hinder SJ, Polychronopoulou K, Yentekakis IV, Goula MA. **An in Depth Investigation of Deactivation through Carbon Formation During the Biogas Dry Reforming Reaction for Ni Supported on Modified with Ceo2 and La2o3 Zirconia Catalysts**. *International Journal of Hydrogen Energy* 2018;**43**(41):18955-18976.

[5] Pham CQ, Cao ANT, Phuong PT TT, Trinh TH Vo DVN, Bui TPT NT. **Enhancement of Syngas Production from Dry Reforming of Methane over Co/Al2o3 Catalyst: Insight into the Promotional Effects of Europium and Neodymium**. *Journal of the Energy Institute* 2022;**105**:314-322.

[6] Zhang X, Xu Y, Liu Y, Niu L DY, Gao Z, Chen B, Xie J, Bi M, Wang M, Xiao D. **A Novel Ni–Mocxoy Interfacial Catalyst for Syngas Production Via the Chemical Looping Dry Reforming of Methane**. *Chem* 2023;**9**(1):102-116.

[7] Usman M, Daud WW, Abbas HF. **Dry Reforming of Methane: Influence of Process Parameters—a Review**. *Renewable and Sustainable Energy Reviews* 2015;**45**:710-744.

[8] Vora B, Chen JQ, Bozzano A, Glover B, Barger P. **Various Routes to Methane Utilization—Sapo-34 Catalysis Offers the Best Option**. *Catalysis Today* 2009;**141**(1-2):77-83.

[9] Sun L, Wang Y, Guan N, Li L. **Methane Activation and Utilization: Current Status and Future Challenges**. *Energy Technology* 2020;**8**(8):1900826.

[10] Benguerba Y, Virginie M, Dumas C, Ernst B. **Methane Dry Reforming over Ni-CO/Al2O3: Kinetic Modelling in a Catalytic Fixed-Bed Reactor**. *International Journal of Chemical Reactor Engineering* 2017;**15**(6) :20160170.

[11] Aghamohammadi S, Haghighi M, Maleki M, Rahemi N. **Sequential Impregnation Vs. Sol-Gel Synthesized Ni/Al2o3-Ceo2 Nanocatalyst for Dry Reforming of Methane: Effect of Synthesis Method and Support Promotion**. *Molecular Catalysis* 2017;**431**:39-48.

[12] Das S AJ, Bian Z, Dewangan N, Wai MH, Du Y, Borgna A, Hidajat K, Kawi S. **Silica–Ceria Sandwiched Ni Core–Shell Catalyst for Low Temperature Dry Reforming of Biogas: Coke Resistance and Mechanistic Insights**. *Applied Catalysis B: Environmental* 2018;**230**:220-236.

[13] Bao Z, Yu F. **Catalytic Conversion of Biogas to Syngas Via Dry Reforming Process**. *Advances in Bioenergy* 2018;**3**:43-76.

[14] Horváth A GL, Kocsonya A,, Sáfrán G LPV, Liotta LF, Pantaleo G, Venezia AM. **Sol-Derived Auni/Mgal2o4 Catalysts: Formation, Structure and Activity in Dry Reforming of Methane**. *Applied Catalysis A: General* 2013;**468**:250-259.

[15] Carapellucci R, Giordano L. **Steam, Dry and Autothermal Methane Reforming for Hydrogen Production: A Thermodynamic Equilibrium Analysis**. *Journal of Power Sources* 2020;**469**:228391.

[16] Vizcaíno A, Lindo M, Carrero A, Calles J. **Hydrogen Production by Steam Reforming of Ethanol Using Ni Catalysts Based on Ternary Mixed Oxides Prepared by Coprecipitation**. *International Journal of Hydrogen Energy* 2012;**37**(2):1985-1992.

[17] Deng J BK, Shen Y, Zhang X, Zhang J, Faungnawakij K, Zhang D. **Cooperatively Enhanced Coking Resistance Via Boron Nitride Coating over Ni-Based Catalysts for Dry Reforming of Methane**. *Applied Catalysis B: Environmental* 2022;**302**:120859.

[18] binti Rosdin RD, Yusuf M, Abdullah B. **Dry Reforming of Methane over Ni-Based Catalysts: Effect of Zro2 and Mgo Addition as Support**. *Materials Letters: X* 2021;**12**:100095, (1-6).

[19] Al-Fatesh AS KR, Fakeeha AH, Kasim SO, Khatri J, Ibrahim AA, Arasheed R, Alabdulsalam M, Lanre MS, Osman AI. **Promotional Effect of Magnesium Oxide for a Stable Nickel-Based Catalyst in Dry Reforming of**

Methane. *Scientific Reports* 2020;**10**(1):13861, (1-10).

[20] Sayari AJCoM. **Catalysis by Crystalline Mesoporous Molecular Sieves**. *Chemistry of Materials* 1996;**8**(8):1840-1852.

[21] Guo M, Wang H, Huang D, Han Z, Li Q WX, Chen J. **Amperometric Catechol Biosensor Based on Laccase Immobilized on Nitrogen-Doped Ordered Mesoporous Carbon (N-Omc)/Pva Matrix**. *Science and Technology of Advanced Materials* 2014;**15**(3): 035005, (1-9).

[22] Elhaj E WH, Al-Harthi EA, Wani WA, Sallam S, Zouli N, Imran M. **Sodium Methoxide Catalysed One-Pot Glycidol Synthesis Via Trans-Esterification between Glycerol and Dimethyl Carbonate**. *Catalysts* 2023;**13**(5):809, (1-10).

[23] Zhang H, Sui S, Zheng X, Cao R, Zhang P. **One-Pot Synthesis of Atomically Dispersed Pt on Mno2 for Efficient Catalytic Decomposition of Toluene at Low Temperatures**. *Applied Catalysis B: Environmental* 2019;**257**:117878.

[24] Liu W, Li L, Zhang X, Wang Z, Wang X PH, Peng H. **Design of Ni-Zro2@ Sio2 Catalyst with Ultra-High Sintering and Coking Resistance for Dry Reforming of Methane to Prepare Syngas**. *Journal of CO2 Utilization* 2018;**27**:297-307.

[25] Gaddalla AM, Sommer ME. **Carbon Dioxide Reforming of Methane on Nickel Catalysts**. *Chemical Engineering Science* 1989;**44**(12):2825-2829.

[26] Barroso Quiroga MM, Castro Luna AE. **Kinetic Analysis of Rate Data for Dry Reforming of Methane**. *Industrial & Engineering Chemistry Research* 2007;**46**(16):5265-5270.

[27] Wei J, Iglesia E. **Structural Requirements and Reaction Pathways in Methane Activation and Chemical Conversion Catalyzed by Rhodium**. *Journal of Catalysis* 2004;**225**(1):116-127.

[28] Bradford MC, Vannice MA. **Co2reforming of Ch4over Supported Pt Catalysts**. *Journal of Catalysis* 1998;**173**(1):157-171.

[29] Wei J, Iglesia E. **Isotopic and Kinetic Assessment of the Mechanism of Reactions of Ch4 with Co2 or H2o to Form Synthesis Gas and Carbon on Nickel Catalysts**. *Journal of Catalysis* 2004;**224**(2):370-383.

[30] Caravella A, Brunetti A, Grandinetti M, Barbieri G. **Dry Reforming of Methane in a Pd-Ag Membrane Reactor: Thermodynamic and Experimental Analysis**. *ChemEngineering* 2018;**2**(4):48, (1-17).

[31] Bradford M, Vannice M. **Co2 Reforming of Ch4**. *Catalysis Reviews* 1999;**41**(1):1-42.

[32] Bradford MC, Vannice MA. **Co2reforming of Ch4over Supported Ru Catalysts**. *Journal of Catalysis* 1999;**183**(1):69-75.

[33] Fogler HS, Gürmen M. **Elements of Chemical Reaction Engineering**. 3rd ed., Mexico: Pearson Educación; 1999.

[34] Fogler HS. **Elements of Chemical Reaction Engineering**. 6th ed., London: Pearson Boston; 2020.

[35] Li P, Yu Y, Huang PP, Liu H, Cao CY SW, Song WG. **Core–Shell Structured Mgal-Ldo@ Al-Ms Hexagonal Nanocomposite: An All Inorganic Acid–Base Bifunctional Nanoreactor for One-Pot Cascade Reactions**. *Journal of Materials Chemistry A* 2014;**2**(2):339-344.

[36] Zhang J, Xin Z, Meng X, Lv Y, Tao M. **Effect of Moo3 on the Heat Resistant Performances of Nickel Based Mcm-41 Methanation Catalysts**. *Fuel* 2014;**116**:25-33.

[37] Barbosa TSB, Barros TRB, Barbosa TLA, Rodrigues MGF. **Green Synthesis for Mcm-41 and Sba-15 Silica Using the Waste Mother Liquor**. *Silicon* 2022;**14**(11):6233-6243.

[38] Sukri MFF, Khavarian M, Mohamed AR. **Effect of Cobalt Loading on Suppression of Carbon Formation in Carbon Dioxide Reforming of Methane over Co/Mgo Catalyst**. *Research on Chemical Intermediates* 2018;**44**:2585-2605.

[39] Dou J, Zhang R, Hao X BZ, Wu T, Wang B, Yu F. **Sandwiched Sio2@ Ni@ Zro2 as a Coke Resistant Nanocatalyst for Dry Reforming of Methane**. *Applied Catalysis B: Environmental* 2019; **254**: 612-623.

[40] Yang M, Lingjun Z, Xiaonan Z, Prasert R, Shurong W. **Co2 Methanation over Nickel-Based Catalysts Supported on Mcm-41 with in Situ Doping of Zirconium**. *Journal of CO2 Utilization* 2020;**42**:101304.

[41] Zhang X, Zhang M, Zhang J, Zhang Q TN, Tan Y, Han Y. **Methane Decomposition and Carbon Deposition over Ni/Zro2 Catalysts: Comparison of Amorphous, Tetragonal, and Monoclinic Zirconia Phase**. *International Journal of Hydrogen Energy* 2019;**44**(33):17887-17899.

[42] Al-Othman ZA. *Synthesis, Modification, and Application of Mesoporous Materials Based on Mcm-41*. Ph.D. Thesis. Oklahoma State University; Stillwater, USA: 2006.

[43] Narasimharao K, Ali TT, Bawaked S, Basahel S. **Effect of Si Precursor on Structural and Catalytic Properties of Nanosize Magnesium Silicates**. *Applied Catalysis A: General* 2014;**488**:208-218.

[44] Wang Yue, Guo Wanqian, Hong-Wei Y, Ho Shih-Hsin, Lo Yung-Chung CC-L, Ren Nanqi, Chang Jo-Shu. **Cultivation of Chlorella Vulgaris Jsc-6 with Swine Wastewater for Simultaneous Nutrient/Cod Removal and Carbohydrate Production**. *Bioresource Technology* 2015;**198**:619-625.

[45] Taherian Z, Khataee A, Orooji Y. **Facile Synthesis of Yttria-Promoted Nickel Catalysts Supported on Mgo-Mcm-41 for Syngas Production from Greenhouse Gases**. *Renewable and Sustainable Energy Reviews* 2020;**134**:110130.

[46] Song Da Hye, Jung Un Ho, Kim Young Eun, Im Hyo Been, Lee Tae Ho L, Ki Bong, Koo Kee Young. **Influence of Supports on the Catalytic Activity and Coke Resistance of Ni Catalyst in Dry Reforming of Methane**. *Catalysts* 2022;**12**(2):216, (1-13).

[47] Lou Y, Steib M, Zhang Q, Tiefenbacher K, Horváth A JA, Liu Y, Lercher JA, Jentys A, Liu Y, Lercher JA. **Design of Stable Ni/Zro2 Catalysts for Dry Reforming of Methane**. *Journal of Catalysis* 2017;**356**:147-156.

[48] Ni J, Chen L, Lin J, Schreyer MK, Wang Z KS. **High Performance of Mg–La Mixed Oxides Supported Ni Catalysts for Dry Reforming of Methane: The Effect of Crystal Structure**. *International Journal of Hydrogen Energy* 2013;**38**(31):13631-13642.

[49] Xie T, Zhao X, Zhang J, Shi L, Zhang D. **Ni Nanoparticles Immobilized Ce-Modified Mesoporous Silica Via a Novel Sublimation-Deposition Strategy for Catalytic Reforming of Methane with Carbon Dioxide**. *International Journal of Hydrogen Energy* 2015;**40**(31):9685-9695.

[50] Zhang Y, Zhang G, Liu J, Li T WY, Zhao Y, Li G, Zhang Y. **Dry Reforming of Methane over Ni/Sio2 Catalysts: Role of Support Structure Properties**. *Fuel* 2023;**340**:127490.

[51] Ekeoma BC, Yusuf M, Johari K, Abdullah B. **Mesoporous Silica Supported Ni-Based Catalysts for Methane Dry Reforming: A Review of Recent Studies**. *International Journal of Hydrogen Energy* 2022;**47**(98):41596-41620.

[52] Sun Y, Zhang G, Cheng H, Liu J, Li G. **Kinetics and Mechanistic Studies of Methane Dry Reforming over Ca Promoted 1co–1ce/Ac-N Catalyst**. *International Journal of Hydrogen Energy* 2021;**46**(1):531-542.

[53] Vertis CS, Oliveira NM, Bernardo FP. **Systematic Development of Kinetic Models for Systems Described by Linear Reaction Schemes**. *Computer Aided Chemical Engineering* 2015; **37**:647-652.

[54] Al-Fatesh AS, Kumar R, Kasim SO, Ibrahim AA, Fakeeha AH, Abasaeed AE, Atia H, Armbruster U, Kreyenschulte C, Lund H, Bartling S. **Effect of Cerium Promoters on an Mcm-41-Supported Nickel Catalyst in Dry Reforming of Methane**. *Industrial & Engineering Chemistry Research* 2021;**61**(1):164-174.

[55] Fogler H. **Elements of Chemical Reaction**. 6th ed., New Jersey: Pearson Education International; 2020.

[56] Wang W-Y, Liu J-H, Lv C-Q, Ren R-R, Wang G-C. **Dry Reforming of Methane on Ni (1 1 1) Surface with Different Mo Doping Ratio: Dft-Assisted Microkinetic Study**. *Applied Surface Science* 2022;**581**:152310.

[57] Li Y, Zhang X, Gao S, Guo W, Liu Z, Wu L, Zheng L, Ding X, Yan H, Wang, Y. **Synthesis of the Ceo2 Support with a Honeycomb-Lantern-Like Structure and Its Application in Dry Reforming of Methane Based on the Surface Spatial Confinement Strategy**. *The Journal of Physical Chemistry C* 2023;**127**(2):1032-1048.

[58] Knoll AJ, Luan P, Pranda A, Bruce RL, Oehrlein GS. **Polymer Etching by Atmospheric-Pressure Plasma Jet and Surface Micro-Discharge Sources: Activation Energy Analysis and Etching Directionality**. *Plasma Processes and Polymers* 2018;**15**(5):1700217.